Distinguishing quantum from classical oscillations in a driven phase qubit

S N Shevchenko[1,6], **A N Omelyanchouk**[1], **A M Zagoskin**[2,3,4], **S Savel'ev**[2,4] **and Franco Nori**[2,5]

[1] B Verkin Institute for Low Temperature Physics and Engineering, 47 Lenin Ave., 61103 Kharkov, Ukraine
[2] Advanced Science Institute, RIKEN, Wako-shi, Saitama 351-0198, Japan
[3] Department of Physics and Astronomy, The University of British Columbia, Vancouver, BC, V6T 1Z1 Canada
[4] Department of Physics, Loughborough University, Loughborough LE11 3TU, UK
[5] Center for Theoretical Physics, Physics Department, Center for the Study of Complex Systems, The University of Michigan, Ann Arbor, MI 48109-1040, USA
E-mail: sshevchenko@ilt.kharkov.ua

Abstract. Rabi oscillations are coherent transitions in a quantum two-level system under the influence of a resonant drive, with a much lower frequency dependent on the perturbation amplitude. These serve as one of the signatures of quantum coherent evolution in mesoscopic systems. It was shown recently (Grønbech-Jensen N and Cirillo M 2005 *Phys. Rev. Lett.* **95** 067001) that in phase qubits (current-biased Josephson junctions) this effect can be mimicked by classical oscillations arising due to the anharmonicity of the effective potential. Nevertheless, we find *qualitative* differences between the classical and quantum effects. Firstly, while the quantum Rabi oscillations can be produced by the subharmonics of the resonant frequency ω_{10} (multiphoton processes), the classical effect also exists when the system is excited at the overtones, $n\omega_{10}$. Secondly, the shape of the resonance is, in the classical case, characteristically asymmetric, whereas quantum resonances are described by symmetric Lorentzians. Thirdly, the anharmonicity of the potential results in the negative shift of the resonant frequency in the classical case, in contrast to the

---

[6] Author to whom any correspondence should be addressed.

IOP Institute of Physics Φ DEUTSCHE PHYSIKALISCHE GESELLSCHAFT

positive Bloch–Siegert shift in the quantum case. We show that in the relevant range of parameters these features allow us to distinguish confidently the bona fide Rabi oscillations from their classical Doppelgänger.

Contents

1. Introduction

Superconducting phase qubits [1, 2] provide a clear demonstration of quantum coherent behaviour in macroscopic systems. They also have a very simple design: a phase qubit is a current-biased Josephson junction (see figure 1(a)), and its working states $|0\rangle$, $|1\rangle$ are the two lowest metastable energy levels $E_{0,1}$ in a local minimum of the washboard potential. The transitions between these levels are produced by applying an RF signal at a resonant frequency $\omega_{10} = (E_1 - E_0)/\hbar \equiv \Delta E/\hbar$. The readout utilizes the fact that the decay of a metastable state of the system produces an observable reaction: a voltage spike in the junction or a flux change in a coupled dc SQUID. In the three-level readout scheme (figure 1(b)), both $|0\rangle$ and $|1\rangle$ have negligible decay rates. A pulse at a frequency $\omega_{21} = (E_2 - E_1)/\hbar$ transfers the probability amplitude from the state $|1\rangle$ to the fast-decaying state $|2\rangle$. Its decay corresponds to a single-shot measurement of the qubit in state $|1\rangle$. Alternatively, instead of an RF readout pulse one can apply a dc pulse, which increases the decay rate of $|1\rangle$.

One of the effects observed in driven phase qubits is Rabi oscillations [2, 3]: coherent transitions in a quantum two-level system under the influence of a resonant perturbation, with a much lower frequency dependence on the perturbation amplitude A via $\Omega_R = \sqrt{A^2 + \delta^2}$, where $\delta = \omega - \omega_{10}$ is the detuning of the driving frequency ω from the resonance frequency ω_{10}. In resonance, $\Omega_R = A$. Multiphoton Rabi oscillations, at $\omega_{10} = n\omega$ (n stands for an integer), observed in such qubits [4, 5], were also interpreted as a signature of coherence.

The quantum coherent dynamics in phase qubits was tested by several complementary methods (see, e.g., [3], [5]–[7]). In particular, in [6], Rabi oscillations between the ground and excited states of the phase qubit were measured by applying a 25 ns pulse at ω_{10} followed by a measurement pulse at ω_{21}. The probability of finding the system in the upper state oscillated with the amplitude of the resonant signal, as it should in the case of Rabi oscillations. In [7], Rabi oscillations were seen instead as the resonant pulse duration varied; a dc readout was used.

However, it is known that the quantum mechanical behaviour of a quantum two-level system can still be similar to the dynamical behaviour of the classical nonlinear oscillator [8]–[13]. In particular, it was recently pointed out [14, 15] that due to the nonlinear behaviour of current-biased Josephson junctions, a similar effect can arise in a purely classical way. Though direct tests—à la Bell—to determine whether a given system is quantum or not
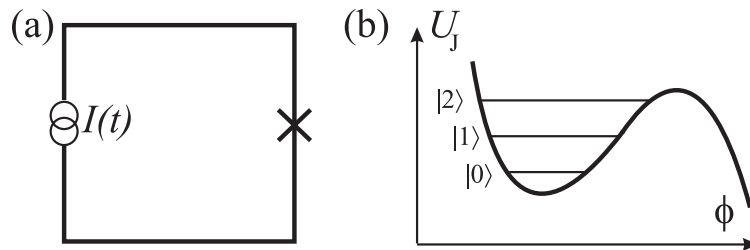
Figure 1. Phase qubit (a) and its Josephson energy (b). The metastable states $|0\rangle$ and $|1\rangle$ can be used as qubit states.

are possible, even their simplified versions (e.g. [13]) are demanding. This motivated us to further investigate the classical behaviour of a phase qubit and find that there is a possibility to distinguish the quantum Rabi oscillations from their classical double, by the shape of the resonance, by the fact that the classical effect can also be produced by the overtones, $n\omega_{10}$, of the resonance frequency, and by the sign of the resonant frequency shift. (An observation that a non-Lorentzian shape of the resonance should exclude a classical explanation has already been made in [16], where the spectroscopy of two coupled qubits was performed. Also, a symmetric versus asymmetric Stark shift in a qubit playing the role of a detector was proposed to distinguish the classical and quantum behaviours of a nanomechanical oscillator [11].) Classical and quantum resonances, as a function of applied drives, are also studied in [17].

2. Model

The phase qubit [1, 2] is a current-biased Josephson junction. The Josephson potential, as a function of the phase difference ϕ,

$$U_{\mathrm{J}}(\phi) = -\frac{\hbar I_{\mathrm{c}}}{2e}(\cos\phi + \phi I_{\mathrm{dc}}/I_{\mathrm{c}}), \tag{1}$$

forms local minima, in which the quantized metastable levels serve as the working states of the qubit. Here, I_{c} is the critical current of the junction, and I_{dc} is the static bias current. A perturbation can be produced by applying a time-dependent bias current, $I_{\mathrm{ac}}\sin\omega t$. In the quantum case, the system can be reduced to a two-level model, described by the Hamiltonian [6]

$$\hat{H} = \frac{\Delta E}{2}\sigma_z + \frac{\hbar I_{\mathrm{ac}}\sin\omega t}{\sqrt{2\Delta EC}}(\sigma_x + \chi\sigma_z), \tag{2}$$

where $\sigma_{z,x}$ are Pauli matrices, C is the capacitance of the junction, and $\chi \approx 1/4$ in the relevant range of parameters. One can obtain from here the Rabi oscillations (coherent oscillations of the probability of finding the system in the upper/lower state with the frequency Ω_{R}) when excited near the resonance or at its subharmonics; the shape of the resonance is a symmetric Lorentzian, as determined by, e.g., the average energy of the system versus the driving frequency ω.

Unlike the flux qubit [18, 19], where the interlevel distance ΔE is determined by the tunnelling, here ΔE is close to the 'plasma' frequency $\omega_{\mathrm{p}} = [2eI_{\mathrm{c}}/\hbar C]^{1/2}$ of small oscillations near the local minima of the potential, equation (1): characteristically $\Delta E/\hbar \approx 0.95\omega_{\mathrm{p}}$ [2]. The same frequency determines the resonance in the system in the classical regime. This means

that, in principle, the same ac signal could cause either the Rabi oscillations or their classical double [14].

3. Classical regime

In the classical regime, the phase qubit can be described by the RSJJ (resistively shunted Josephson junction) model [20, 21], in which the equation of motion for the superconducting phase difference across the junction, characterized by the normal (quasiparticle) resistance R, reads

$$\frac{\hbar C}{2e}\frac{\mathrm{d}^2\phi}{\mathrm{d}t^2} + \frac{\hbar}{2eR}\frac{\mathrm{d}\phi}{\mathrm{d}t} + I_\mathrm{c}\sin\phi = I_\mathrm{dc} + I_\mathrm{ac}\sin\omega t. \tag{3}$$

Introducing the dimensionless variables,

$$\tau = \omega_\mathrm{p} t, \quad \gamma = \omega/\omega_\mathrm{p}, \tag{4}$$

we obtain

$$\ddot{\phi} + \alpha\dot{\phi} + \sin\phi = \eta + \epsilon\sin\gamma\tau, \tag{5}$$

where

$$\alpha = \frac{\hbar\omega_\mathrm{p}}{2eRI_\mathrm{c}}, \qquad \eta = \frac{I_\mathrm{dc}}{I_\mathrm{c}}, \qquad \epsilon = \frac{I_\mathrm{ac}}{I_\mathrm{c}}, \tag{6}$$

and the dot stands for the derivative with respect to τ. The solution is sought in the phase-locked ansatz,

$$\phi(\tau) = \phi_0 + \psi(\tau), \quad \psi \ll 1. \tag{7}$$

We substitute equation (7) into (5) and expand $\sin\phi$ to third order, which yields

$$\ddot{\psi} + \alpha\dot{\psi} + \psi\cos\phi_0 = \eta - \sin\phi_0 + \frac{\sin\phi_0}{2}\psi^2 + \frac{\cos\phi_0}{6}\psi^3 + \epsilon\sin\gamma\tau. \tag{8}$$

Therefore, $\sin\phi_0 = \eta$, and by introducing

$$\gamma_0 = [1 - \eta^2]^{1/4}, \tag{9}$$

we obtain

$$\ddot{\psi} + \alpha\dot{\psi} + \gamma_0^2\psi = \epsilon\sin\gamma\tau + \frac{\eta}{2}\psi^2 + \frac{\gamma_0^2}{6}\psi^3, \tag{10}$$

which describes the anharmonic driven oscillator [22].

Here, we briefly point out several features of the solution of equation (10) (for more details see chapter 5 in [22]).

(i) The anharmonic driven oscillator, described by equation (10), is resonantly excited at any frequency $\gamma \approx \frac{p}{q}\gamma_0$, where p and q are integers. This however happens in higher approximation in the driven amplitude ϵ. At a small amplitude ϵ, the most pronounced resonances appear at $\gamma \approx \gamma_0$ (main resonance), $\gamma \approx \gamma_0/2$ (anharmonic-type resonance) and $\gamma \approx 2\gamma_0$ (parametric-type resonance).

(ii) The amplitude b of the small driven oscillations at the main resonance is $b_{\max} = \epsilon/(\gamma_0 \alpha)$. When this amplitude is not small, the phase-locked ansatz becomes invalid. Then the solution of equation (5) describes the escape from the phase-locked state, which means the appearance of a nonzero average voltage on the contact. This voltage is proportional to the average derivative of the phase, $\bar{\dot{\phi}}$.

(iii) The position of the resonances for small oscillations is shifted due to the anharmonicity of the potential. This, for the main resonance γ_{res}, is given by:

$$\gamma_{\mathrm{res}} - \gamma_0 = \varkappa b^2, \tag{11}$$

$$\varkappa = -\frac{3 + 2\eta^2}{48\gamma_0^3}. \tag{12}$$

Note that the resonance shift is negative (e.g. as in [11]).

(iv) The shape of the resonances, as a function of the driven frequency γ, is essentially non-symmetrical. The asymmetry of the main resonance becomes pronounced at

$$\epsilon \gtrsim \frac{\gamma_0 \alpha^{3/2}}{|\varkappa|^{1/2}}, \tag{13}$$

at small enough damping.

(v) The parametric-type resonance at $\gamma \approx 2\gamma_0$ appears when the damping is sufficiently low, i.e. at

$$\alpha < \frac{\eta \epsilon}{6\gamma_0^3}. \tag{14}$$

At the relevant parameters, $\eta \simeq 0.9$, $\gamma_0 \simeq 0.6$, this means the following:

$$\frac{\epsilon}{\gamma_0 \alpha} > \frac{6\gamma_0^2}{\eta} \simeq 2, \tag{15}$$

which is fulfilled (see (ii)) when the solution close to the main resonance corresponds to the escape from the phase-locked state.

We note that for the anharmonic driven oscillator, described by equation (10), both the resonances at $\gamma_0/2$ and $2\gamma_0$ appear due to the anharmonicity of the potential energy and are of the same order. For the driven flux qubit in the classical regime [19], the equation for the phase variable $\theta(t) = \theta_0 + \psi(t)$ can also be expanded for small oscillations $\psi(t)$ about the value θ_0; restricting ourselves here to the linear in ψ terms, the equation can be rewritten in the form:

$$\ddot{\psi} + \alpha \dot{\psi} + \gamma_0^2[1 - h \sin \gamma \tau]\psi = \epsilon \sin \gamma \tau. \tag{16}$$

In this case, the genuine parametric resonance at $\gamma \approx 2\gamma_0$ appears due to the term containing $\sin \gamma \tau \cdot \psi$ [22]. This explains the prevailing of this resonance over the resonance at $\gamma \approx \gamma_0/2$, due to the small anharmonicity of the potential in [19].

Now we proceed to numerically solve the equation of motion (5) for the relevant set of parameters close to the experimental case. We also investigate the behaviour of the energy of the system [20, 21]

$$H = \tfrac{1}{2}\dot{\phi}^2 + 1 - \cos\phi - (\eta + \epsilon \sin \gamma \tau)\phi, \tag{17}$$

which determines the thermally activated escape probability from the local minimum of the potential [23] in equation (1). The classical Rabi-like oscillations are displayed in figure 2.
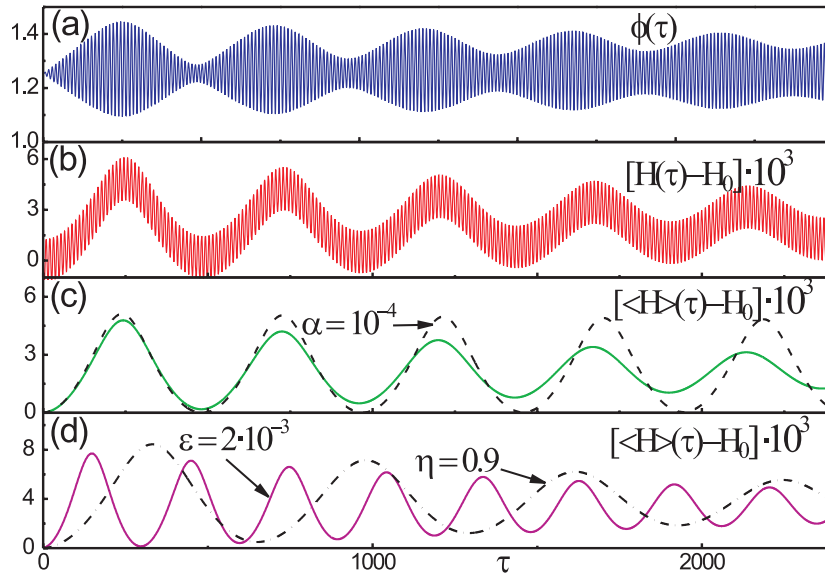
Figure 2. Rabi-type oscillations in current-biased Josephson junctions: (a) and (b) show the time dependence of the phase difference ϕ and of the energy H, respectively; (c) presents the time dependence of the energy, averaged over the fast oscillations with period $2\pi/\omega$. All energies are shifted by their stationary value: $H_0 = 1 - \sqrt{1 - \eta^2} - \eta \arcsin \eta$. The parameters for the blue, red and green curves are $\eta = 0.95$, $\alpha = 10^{-3}$, $\epsilon = 10^{-3}$ and $\gamma = \gamma_0$; for the other curves in (c) and (d), only one parameter was different from the above, for comparison, namely: (c) dashed black line, $\alpha = 10^{-4}$; (d) solid violet line, $\epsilon = 2 \times 10^{-3}$; dashed–dotted black line, $\eta = 0.9$.

In figure 2(a), the modulated transient oscillations of the phase difference ϕ are plotted. These oscillations result in the oscillating behaviour of the energy of the system as shown in figure 2(b). Averaging over fast oscillations, we plot in figure 2(c) with a green solid curve the damped oscillations of the energy, analogous to the quantum Rabi oscillations [14]. These curves are plotted for the following set of the parameters: $\eta = 0.95$, $\alpha = 10^{-3}$, $\epsilon = 10^{-3}$ and $\gamma = \gamma_0$. For comparison we also plotted the energy averaged over the fast oscillations for different parameters, changing one of these parameters and leaving the others the same. The dashed black curve in figure 2(c) is for the smaller damping, $\alpha = 10^{-4}$; the solid (violet) line and the dashed–dotted (black) line in figure 2(d) demonstrate the change in the frequency and the amplitude of the oscillations, respectively, for $\epsilon = 2 \times 10^{-3}$ and $\eta = 0.9$. We notice that the effect analogous to the classical Rabi oscillations exists in a wide range of parameters.

In figure 3, the effect of the driving current on the time-averaged energy of the system is shown for different driving amplitudes: figure 3(a) for weaker amplitudes, close to the main resonance, to show the asymmetry and negative shift of the resonance; and figure 3(b) for stronger amplitudes, to show the resonances at $\gamma_0/2$ and $2\gamma_0$ (which are also shown enlarged in the insets). We note that the parametric-type resonance at $2\gamma_0$ originates from the third-order terms when the solution of the equation for ψ is sought by iterations [22]; when there are two or more terms responsible for this resonance, the respective resonance may become split, which is visible in figure 3(b) for the lowest curve. An analogous tiny splitting of the resonance was obtained for the driven flux qubit in figure 4 of [19].
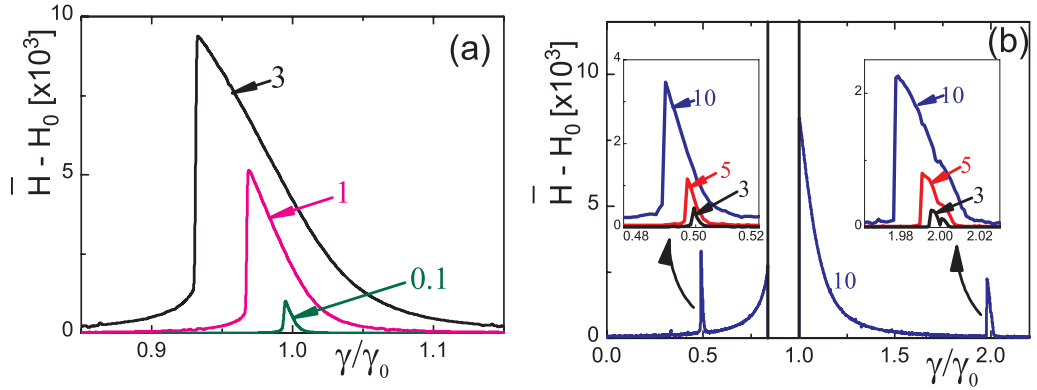
Figure 3. The time-averaged energy $\bar{H} - H_0$ versus reduced frequency for relatively weak (a) and strong (b) driving. Different values of the driving amplitude ϵ (multiplied by 10^3) are shown by the numbers next to the curves. The parameters are: $\eta = 0.95$ and $\alpha = 10^{-4}$. In (b), the region between the vertical black lines corresponds to the escape from the phase-locked state.
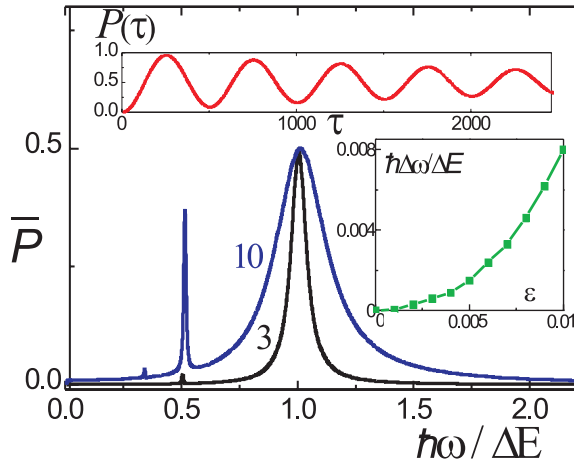

Figure 4. The time-averaged probability $\bar{P}$ of the upper level to be occupied versus the driving frequency. The parameters used here are: $\eta = 0.95$, $E_J/\hbar\omega_p = 300$, $\Gamma_{\text{relax}}/\hbar\omega_p = \Gamma_\phi/\hbar\omega_p = 3 \times 10^{-4}$. Numbers next to the curves stand for ϵ multiplied by 10^3. Upper inset: the time dependence of the probability $P(\tau)$. Right inset: the shift of the principal resonance (at $\hbar\omega \approx \Delta E$), where $\Delta\omega = \omega - \Delta E/\hbar$.

4. Quantum regime

In the quantum regime, the phase qubit can be described by the Bloch equations for the density matrix components. In order to take into account the relaxation and dephasing processes, the corresponding rates $\Gamma_{\text{relax}} \equiv \hbar\omega_p \cdot \lambda_{\text{relax}}$ and $\Gamma_\phi \equiv \hbar\omega_p \cdot \lambda_\phi$ are included in the Liouville equation phenomenologically [24]. Then the evolution of the reduced density matrix $\hat{\rho}$, taken in the form

$$\hat{\rho} = \frac{1}{2}\begin{bmatrix} 1+Z & X-iY \\ X+iY & 1-Z \end{bmatrix}, \tag{18}$$

IOP Institute of Physics Φ DEUTSCHE PHYSIKALISCHE GESELLSCHAFT

is described by the Bloch equations [24, 25]:

$$\dot{X} = -CY - \lambda_\phi X, \tag{19}$$

$$\dot{Y} = -AZ + CX - \lambda_\phi Y, \tag{20}$$

$$\dot{Z} = AY - \lambda_{\text{relax}}(Z - Z_0), \tag{21}$$

where A and C stand for the off-diagonal and diagonal parts of the dimensionless Hamiltonian:

$$\frac{\hat{H}}{\hbar\omega_p} = \frac{\Delta E}{2\hbar\omega_p}\sigma_z + \frac{\hbar I_{\text{ac}}\sin\omega t}{\hbar\omega_p\sqrt{2\Delta EC}}(\sigma_x + \chi\sigma_z) \equiv \frac{A}{2}\sigma_x + \frac{C}{2}\sigma_z. \tag{22}$$

From these equations we obtain $Z(\tau)$, which defines the occupation probability of the upper level,

$$P(\tau) = \rho_{22}(\tau) = \tfrac{1}{2}(1 - Z(\tau)). \tag{23}$$

We choose the initial condition to be $X(0) = Y(0) = 0$, $Z(0) = 1$, which corresponds to the system being in the ground state; we also consider the zero-temperature limit in which the equilibrium value of Z is $Z_0 = 1$.

When the system is driven close to resonance, $\omega \approx \Delta E$, the upper level occupation probability $P(\tau)$ exhibits Rabi oscillations. The damped Rabi oscillations are demonstrated in the upper inset in figure 4, which is analogous to the classical oscillations presented in figure 2. After averaging the time-dependent probability, we plot it versus frequency in figure 4 for two values of the amplitude, demonstrating the multiphoton resonances. Figure 4 demonstrates the following features of the multiphoton resonances in the quantum case: (a) in contrast to the classical case, the resonances appear only at the subharmonics, at $\hbar\omega \approx \Delta E/n$; (b) the resonances have Lorentzian shapes (as opposed to the classical asymmetric resonances); (c) with increasing the driving amplitude, the resonances shift to the higher frequencies—the Bloch–Siegert shift, which has the opposite sign to that of its classical counterpart. The Bloch–Siegert shift (the shift of the principal resonance at $\hbar\omega \approx \Delta E$) is plotted numerically in the right inset in figure 4. Analogous shifts of the positions of the resonances were recently observed experimentally [5].

5. Conclusions

In conclusion, the following criteria can be proposed to distinguish classical Rabi-type oscillations in current-biased Josephson junctions: (i) the appearance of resonances both at the overtones of the main resonant frequency (e.g. $2\gamma_0$) and its subharmonic ($\gamma_0/2$); (ii) the asymmetric shape of the resonances; and (iii) a negative shift of the resonant frequency when increasing the driving amplitude. In recent publications, these features were not reported: multiphoton resonances were observed [4, 5]; the resonances observed have a Lorentzian shape [3, 16][7] and have a positive frequency shift [5], which means that the observed resonant excitations in the system were in the *quantum* regime.

---

[7] We note in passing that in other types of qubits the Lorentzian-shaped multiphoton resonances were also observed [26]–[30].

IOP Institute of Physics **⊕** DEUTSCHE PHYSIKALISCHE GESELLSCHAFT

Acknowledgments

References

[1] You J Q and Nori F 2005 *Phys. Today* **58** (11) 42
[2] Martinis J, Nam S, Aumentado J and Urbina C 2002 *Phys. Rev. Lett.* **89** 117901
[3] Claudon J, Balestro F, Hekking F W J and Buisson O 2004 *Phys. Rev. Lett.* **93** 187003
[4] Wallraff A, Duty T, Lukashenko A and Ustinov A V 2003 *Phys. Rev. Lett.* **90** 037003
[5] Strauch F W *et al* 2007 *IEEE Trans. Appl. Supercond.* **17** 105
[6] Martinis J M, Nam S, Aumentado J, Lang K M and Urbina C 2003 *Phys. Rev.* B **67** 094510
[7] Lisenfeld J, Lukashenko A, Ansmann M, Martinis J M and Ustinov A V 2007 *Phys. Rev. Lett.* **99** 170504
[8] Spreeuw R J C, van Druten N J, Beijersbergen M W, Eliel E R and Woerdman J P 1990 *Phys. Rev. Lett.* **65** 2642
[9] Zhu Y, Gauthier D J, Morin S E, Wu Q, Carmichael H J and Mossberg T W 1990 *Phys. Rev. Lett.* **64** 2499
[10] Peano V and Thorwart M 2004 *Phys. Rev.* B **70** 235401
[11] Wei L F, Liu Y X, Sun C P and Nori F 2006 *Phys. Rev. Lett.* **97** 237201
[12] Rotoli G, Bauch T, Lindstrom T, Stornaiuolo D, Tafuri F and Lombardi F 2007 *Phys. Rev.* B **75** 144501
[13] Alicki R and Van Ryn N 2008 *J. Phys. A: Math. Theor.* **41** 062001
[14] Grønbech-Jensen N and Cirillo M 2005 *Phys. Rev. Lett.* **95** 067001
[15] Marchese J E, Cirillo M and Grønbech-Jensen N 2007 *Open Systems and Information Dynamics* **14** 189
[16] Berkley A J, Xu H, Ramos R C, Gubrud M A, Strauch F W, Johnson P R, Anderson J R, Dragt A J, Lobb C J and Wellstood F C 2003 *Science* **300** 1548
[17] Savel'ev S, Hu X and Nori F 2006 *New J. Phys.* **8** 105
Savel'ev S, Rakhmanov A L, Hu X, Kasumov A and Nori F 2007 *Phys. Rev.* B **75** 165417
[18] Mooij J E, Orlando T P, Levitov L, Tian L, van der Wal C H and Lloyd S 1999 *Science* **285** 1036
[19] Omelyanchouk A N, Shevchenko S N, Zagoskin A M, Il'ichev E and Nori F 2007 *Preprint* 0705.1768
[20] Likharev K 1986 *Dynamics of Josephson Junctions and Circuits* (New York: Gordon and Breach)
[21] Barone A and Paterno G 1982 *Physics and Applications of the Josephson Effect* (New York: Wiley)
[22] Landau L D and Lifshitz E M 1976 *Mechanics* (Oxford: Pergamon)
[23] Grønbech-Jensen N, Castellano M G, Chiarello F, Cirillo M, Cosmelli C, Merlo V, Russo R and Torrioli G 2006 *Quantum Computing in Solid State Systems* ed B Ruggiero, P Delsing, C Granata, Y Pashkin and P Silvestrini (Berlin: Springer) p 111
[24] Blum K 1981 *Density Matrix Theory and Applications* (New York: Plenum)
[25] Shevchenko S N, Kiyko A S, Omelyanchouk A N and Krech W 2005 *Low Temp. Phys.* **31** 564
[26] Nakamura Y, Pashkin Yu A and Tsai J S 2001 *Phys. Rev. Lett.* **87** 246601

[27] Saito S, Thorwart M, Tanaka H, Ueda M, Nakano H, Semba K and Takayanagi H 2004 *Phys. Rev. Lett.* **93** 037001

[28] Oliver W D, Yu Ya, Lee J C, Berggren K K, Levitov L S and Orlando T P 2005 *Science* **310** 1653

[29] Shnyrkov V I, Wagner Th, Born D, Shevchenko S N, Krech W, Omelyanchouk A N, Il'ichev E and Meyer H-G 2006 *Phys. Rev.* B **73** 024506

[30] Sillanpää M, Lehtinen T, Paila A, Makhlin Yu and Hakonen P 2007 *J. Low Temp. Phys.* **146** 253
Sillanpää M, Lehtinen T, Paila A, Makhlin Yu and Hakonen P 2006 *Phys. Rev. Lett.* **96** 187002